Brief communication: Everest South Col Glacier did not thin during the last three decades

Fanny Brun[1], Owen King[2], Marion Réveillet[1], Charles Amory[1], Anton Planchot[1,3], Etienne Berthier[4], Amaury Dehecq[1], Tobias Bolch[2], Kévin Fourteau[5], Julien Brondex[5], Marie Dumont[5], Christoph Mayer[6], Silvan Leinss[7], Romain Hugonnet[8,9,10], and Patrick Wagnon[1]

[1]Univ. Grenoble Alpes, IRD, CNRS, INRAE, Grenoble INP, IGE, Grenoble, France
[2]Department of Geography and Sustainable Development, University of St Andrews, St Andrews, Scotland, UK
[3]Geosciences Department, École Normale Supérieure - PSL University, Paris, France
[4]LEGOS, Université de Toulouse, CNES, CNRS, IRD, UPS, Toulouse, France
[5]Univ. Grenoble Alpes, Université de Toulouse, Météo-France, CNRS, CNRM, Centre d'Études de la Neige, Grenoble, France
[6]Bavarian Academy of Sciences and Humanities, Geodesy and Glaciology, Munich, Germany
[7]Gamma Remote Sensing AG, 3073 Gümligen, Switzerland
[8]University of Washington, Civil and Environmental Engineering, Seattle, WA, USA
[9]Laboratory of Hydraulics, Hydrology and Glaciology (VAW), ETH Zürich, Zürich, Switzerland
[10]Swiss Federal Institute for Forest, Snow and Landscape Research (WSL), Birmensdorf, Switzerland

Correspondence: Fanny Brun (fanny.brun@univ-grenoble-alpes.fr)

Abstract. The South Col Glacier is ~~an iconic~~ a small body of ice and snow (approx. 0.2 km^2), located on the southern ridge of Mt. Everest. A recent study proposed that South Col Glacier is rapidly losing mass. This ~~seems~~ is in contradiction with our comparison of two digital elevation models derived from aerial photographs taken in December 1984 and a stereo Pléiades satellite acquisition from March 2017, from which we ~~measure~~ estimate a mean elevation change of 0.01 ± ~~0.07~~ 0.05 m a^{-1}. To reconcile these results we investigate wind erosion and surface energy and mass balance, and find that melt is unlikely a dominant process, contrary to previous findings.

1 Introduction

Glaciers and ice caps are losing mass at an accelerated rate in almost all regions on Earth and are icons of climate change (IPCC, 2021; Zemp et al., 2019; Hugonnet et al., 2021). It is generally observed that the lowest parts of glaciers thin at ~~large rates ,~~ rates often exceeding 1 m a^{-1}, with variability between regions and glaciers (Hugonnet et al., 2021). Upper accumulation areas are more stable, with rates of elevation changes often close to zero, even for some high-elevation regions where the warming of the firn column is documented (Vincent et al., 2020).

In the Everest region, glaciers have lost mass at a ~~continuously-accelerating~~ continuously accelerating rate since 1962, reaching a ~~regionally-averaged mass loss~~ regionally averaged mass change rate of -0.38 ± 0.13 m w.e a^{-1} for the period 2009-2018 (King et al., 2020). Thinning for the period 1984-2018 was observed up to elevations of approximately 6000 m a.s.l., and was

close to zero at higher elevations (King et al., 2020). Within this context, a recent study surprisingly suggested substantial thinning of the South Col Glacier, located at 8020 m a.s.l. (Potocki et al., 2022). Based on the interpretation of an ice core and surface energy balance modeling, Potocki et al. (2022) estimated that contemporary thinning rates — or ~~ablation~~ negative surface mass balance rates, because the authors did not consider ice dynamics — were approaching 2 m a^{-1} over the ∼ 1990-2019 period.

The South Col Glacier is a small body of snow and ice, covering an area of approximately 0.2 km^2. It is located on the ascent route of Mt. Everest from Nepal. Despite this iconic location, it is largely without prior scientific investigation, due to the logistical challenge ~~to conduct~~ of conducting scientific fieldwork in this very high altitude environment. ~~It is also a difficult target for remote sensing techniques, being small and subject both to bright snow conditions and persistent cloud coverage during monsoon (occurring in JJAS).~~ Processes governing the surface energy balance of the ice and snow in the extreme high altitude weather remain poorly constrained, despite the installation of an ~~Automatic Weather Station~~ automatic weather station (AWS)~~in~~, which was running between May 2019 and August 2022, with some gaps, on a rock outcrop close to the South Col (Matthews et al., 2020).

Interpreting a shallow ice core (approximately 10 m long) drilled in May 2019 and modeling the surface energy balance, Potocki et al. (2022) concluded that the glacier surface state likely transitioned from a snow-dominated surface to an ~~ice dominated~~ ice-dominated surface in the 1990s, leading to large amounts of melt (averaging to 1.5 m w.e. a^{-1} over the considered period), which was the main cause for the disappearance of ∼55 m of ice over a 30 year period covering 1990 to ~~present.~~ 2019. Based on these observations, Potocki et al. (2022) ~~suggest~~ suggested that Himalayan glaciers at or above 8000 m a.s.l. may not survive beyond the middle of the 21st century.

In this brief communication, we explore the elevation change of South Col Glacier for the period 1984-2017, based on digital elevation model (DEM) differencing. We also ~~explore~~ investigate the processes governing the mass balance of South Col Glacier from satellite images and models in order to compare our findings with those of Potocki et al. (2022).

2 South Col Glacier elevation change

We used aerial photographs and tri-stereo Pleiades data to generate DEMs and investigate surface elevation changes. The Pléiades DEM was generated from imagery acquired on the 23 March 2017 using the Ames Stereo Pipeline software ~~(Shean et al., 2016)~~ (Berthier et al., 2014; Beyer et al., 2018). The 1984 DEM was generated from a subset of images acquired by Bradford Washburn over the wider Everest region on 20 December 1984 using a Wild RC-10 camera (Washburn, 1989) on behalf of the National Geographic Survey. We focus on three images in which the South Col Glacier is located centrally within the frame to avoid peripheral image distortion, and we processed images from a single flight line in the survey to avoid problems associated with DEM merging. The images were produced by scanning of the original diapositives at 1693 dpi which results in a ~~ground~~

50 ~~resolution~~ pixel spacing of 0.5 m. The 1984 DEM was generated using PCI Geomatica with the aid of 10 ground control points (GCPs) extracted from the 2017 Pléiades orthoimage and DEM. ~~Both the Pléiades and aerial photograph DEMs were generated at~~ We used these GCPs, in combination with 90 tie points, which relate ground features visible in overlapping images to one another, to perform a bundle adjustment – the optimisation of camera position and orientation. The root mean square error (RMSE) associated with these 10 GCPs was 0.76, 0.94 and 1.92 m in X, Y and Z directions, following bundle adjustment,

55 suggesting the precise rectification of the 1984 imagery in relation to the reference Pléiades scene. Stereo triangulation between the rectified overlapping images was performed using the semiglobal matching method (Hirschmuller, 2008) resulting in a DEM with 2 m ~~ground resolution~~ posting to match the resolution of the Pléiades DEM.

To ensure the precise coregistration of both DEMs prior to differencing, we removed shifts (all below 2 m) following Nuth and Kääb (2011). We modified the GAMDAM glacier inventory (GG18; Sakai, 2019) over the surroundings of the South

60 Col using the Pleiades orthoimage (~~GGI18) (Sakai, 2019) over the South Col surroundings using the Pléiades high resolution (~~0.5 m) ~~orthoimage. The revised inventory allowed for coregistration of DEMs~~ to delineate glacier boundaries, allowing for DEM co-registration over stable, off-glacier ~~areas, following the methods of Nuth and Kääb (2011)~~surfaces. We also ~~define~~ defined the outlines of South Col Glacier, which is not identified as a single glacier in the original ~~GGI18~~ GG18 inventory (Fig. 1). Following DEM differencing, surface elevation change data (dH) were filtered to remove outliers, with values outside

65 the range of five times the standard deviation of dH estimates within 50 m elevation bands removed below 6800 m a.s.l. Above 6800 m, or from the base of the much steeper Lhotse face, we applied a threshold of three times the standard deviation of dH estimates, as the range of elevation change values ~~were higher here~~ here include high magnitude elevation changes ($\pm \sim 35$ m) associated with crevasse field evolution captured by both DEMs. To fill small data voids we computed a smoothed version of the dH grid where the value of each cell was derived as the mean of a 5x5 cell window, centered on the respective pixel. Data

70 voids in the original dH grid smaller than this window size were then filled with the 'mean' values. ~~Any resulting minor data voids were filled using mean values from surrounding pixels within the dH grid.~~

~~Uncertainty~~ The uncertainty associated with the ~~average~~ mean elevation change over ~~glacier surfaces ($\sigma_{\Delta z,g}$) was established following the methods of Rolstad et al. (2009) and Fischer et al. (2015), whereby:~~ South Col Glacier ($\sigma_{dH,SCG}$) was estimated following Hugonnet et al. (2022). This robust approach applies error propagation for correlated variables considering, in the

75 structure of error, the spatial correlation of errors at multiple ranges modelled by a variogram $\gamma_{z_{dH}}$, and the heteroscedasticity (i.e., variability in error) modelled by a variable variance $\sigma_{dH}^2(\alpha,c)$ that is a function of the terrain slope α and maximum absolute curvature c:

$$\sigma_{\underline{\Delta z,g}dH,SCG}^2 = \overline{\sigma_{dH}^2(\alpha,c)}|_A \frac{1}{N^2} \sum_{i=1}^{N} \sum_{j=1}^{N} \left(1 - \gamma_{z_{dH}}(d_{i,j}) \right), \tag{1}$$

~~where $\sigma_{\Delta h}$ (m) is the standard deviation of dH over stable , off-glacier terrain , $A_{cor} = \pi L^2$, with L being the distance over~~

80 ~~which dH data are spatially correlated (Rolstad et al., 2009), here measured to be 1193 m, and A_g is the area of the glacier.~~

where $\overline{\sigma_{dH}^2(\alpha,c)}\big|_A$ is the average of the variance of elevation differences $\sigma_{dH}^2(\alpha,c)$ in the glacier area A, composed of N pixels. $\sigma_{dH}^2(\alpha,c)$ is inferred by the square of the half-difference between the 0.025 and 0.975 quantiles (a robust proxy for the 2-σ uncertainty range) in binned categories of elevation differences on stable terrain. $\gamma_{z_{dH}}$ is the variogram of the standard score z_{dH} on stable terrain (i.e., elevation differences standardized by $\sigma_{dH}(\alpha,c)$), estimated by a median empirical variogram and modelled by a sum of two spherical models. The variogram of the standard score takes values between 0 (fully correlated) and 1 (uncorrelated) depending on the spatial lag $d_{i,j}$ (i.e. distance between pixel i and j). We found that 89% of the variance is correlated until a first range of 87 m, while the remaining 11% are correlated until a second range of 6.5 km, after which errors are fully decorrelated.

~~Within a 50 m diameter circle centered on the drilling location, the elevation change is 1.7 ± 2.2 m for the period 1984-2017, corresponding~~ Several patterns of dH are evident over the Western Cwm and South Col Glacier surroundings, which relate to both ice flow and surface mass balance processes (Fig. A1). Thinning and recession of the steep hanging glaciers on the north face of the Western Cwm is evident north of Camp II at an elevation of 6500 m a.s.l. (Fig. A1 panels d-f). Slight ($\sim$ 10 m or less) thinning is evident over the Khumbu Glacier up to an elevation ~~change rate of 0.05 ± 0.07 m a^{-1}, meaning that the thickness change is statistically not different from zero~~ of 7000 m a.s.l. Above this height, substantial elevation change is limited to areas where ice flow has driven crevasse field evolution between the two DEM dates, primarily on the Lhotse and Kangshung faces, to the southwest and east of South Col Glacier, respectively (Fig. ~~1~~A1 panels a-c). Over the ~~whole glacier area~~South Col Glacier specifically, we find a mean elevation change of 0.01 ± 0.07 m a^{-1} for the period 1984-2017. The distribution of dH on South Col Glacier is rather homogeneous and not different from the distribution of dH over ice-free areas or over glacierized areas located within the same elevation range (Fig. A2). The distribution of elevation change values off-ice centered around zero (mean of 0.07 m, standard deviation of 3.72 m) gives us confidence in the successful processing of both DEMs in the study area. Within a 50 m diameter circle, centered on the drilling location of Potocki et al. (2022), the elevation change is 1.7 ± 5.1 m for the period 1984-2017, corresponding to an elevation change rate of 0.05 ± 0.15 m a^{-1}. Glacier-wide and local (at drill site) thickness change are thus statistically not different from zero (Fig. 1). This observation can be extended back in the past, at least in a qualitative way, as the comparison of photographs from the Swiss expedition to Everest in 1956 with photographs from 2008 and 2022 shows that there are no large changes visible of the thickness of South Col Glacier (Machguth and Mattea, 2022).

3 Surface mass balance processes

We investigate the mass balance processes to further understand the ~~different~~ contending conclusions between the findings of Potocki et al. (2022) and ~~the non-elevation change result found here~~our observations of no elevation change of South Col Glacier over the last three decades. Little is known about the surface mass balance processes at such high altitude, and consequently, we ~~mobilize multiple methods~~utilize multiple methods and data to investigate them. We first analyze high temporal resolution satellite images to document the seasonal evolution of the glacier surface state. We then model the potential

magnitude of wind erosion, as it could be a very important process (Litt et al., 2019). Finally, we run a surface energy balance model with different configurations to investigate the significance of surface melt.

3.1 Seasonal surface state changes from satellite images

Due to its small size, highly reflective surface and persistent cloud coverage during monsoon season, the South Col Glacier is challenging to observe with standard optical satellite imagery. The VENμS satellite acquired multispectral images every 2 to 30 days from November 2017 to October 2020 that are suitable to qualitatively document the surface state changes of South Col Glacier (e.g., Bessin et al., 2022). VENμS images consist of 12 narrow spectral bands from blue visible (0.424 μm) to near-infrared (0.910 μm), with a 5 m ground resolution, acquired at 11:00 local time (Dick et al., 2022).

We use 267 VENμS surface reflectance (SRE) multispectral images that we crop to the South Col Glacier surroundings. Fourteen images with poor co-registration were horizontally shifted, by manually selecting four GCPs. All other images are well co-registered and orthorectified in the original SRE product. We produce natural color composites using the band combination 7-4-3, corresponding to red, green and blue bands, respectively. The *equalize_adapthist* function from Python *scikit-image* package was used to obtain a rendering that highlights the blue ice areas (Fig. 2). We rely on visual inspection of the images only, and did not attempt to automatically classify the snow covered areas.

The South Col Glacier exhibits strong seasonal contrasts in terms of snow cover. Here we show only one image per month for the year 2019 (Fig. 2), but the whole image series is available (Brun, 2022). From January to June, the glacier surface is partially covered by snow, while ice is exposed in multiple places. The exposed ice area increases, at least until May, and even sometimes June. After mid June, the number of usable images is limited due to monsoon cloud cover, and the only image available in July shows that the glacier is covered by a thin layer of snow, as the ice is visible underneath. The glacier is then covered by an apparently thicker layer of snow in August, September and October. The ice is not visible, except on the lower cliff of South Col Glacier, above the Western Cwm (upper part of Khumbu Glacier, on the west side of South Col Glacier) in October. The ice re-appears in November, and its exposed area increases through the course of December (Fig. 2).

The series of VENμS images shows an excellent qualitative agreement with the albedo series measured at the South Col AWS in 2019 (Matthews et al., 2020). The South Col AWS (purple star on Fig. 2) was installed on a rock outcrop, which became covered by snow in early July 2019. Then the albedo of the surface below the AWS remained high until mid October 2019, when the rock outcrop was re-exposed (Matthews et al., 2020).

With VENμS, we observe only three years (2018, 2019 and 2020), but our findings are similar for the three years. The qualitative interpretation of the VENμS image series hints at a dominant role of wind erosion in the surface mass balance. They show that late monsoon accumulation is removed during subsequent periods as large blue ice areas, starting at the east part of the glacier, become exposed within a few days in October-November when the available energy is limited for melt and when the wind speed is high.

3.2 The ~~quantitative importance~~ potential of wind erosion

In order to test the ~~quantitative~~ importance of wind erosion, we implement a simple model inspired from Amory et al. (2021). ~~For the sake of clarity, the difference between precipitationand erosion is named deposition(and not accumulation).~~ Hereafter we define accumulation as the snow that is deposited to the glacier surface (i.e. a fraction of precipitation) minus the erosion (i.e. the snow that is mechanically removed by wind from the glacier surface after the deposition). Accumulation can thus be negative when erosion exceeds deposition. The parameterization of wind erosion is based on a set of semi-empirical formulations, originally implemented in the polar-oriented regional climate model MAR (Gallée et al., 2001; Amory et al., 2021). MAR has been used to study the cryosphere under various climates, and the erosion/deposition processes have been largely validated in Antarctica where these processes are critical (e.g., Agosta et al., 2019). ~~The cold and windy environment of Antarctic glaciers is also the most similar to high elevation sites such as South Col Glacier.~~ Here we develop a simplified analytical approach expressed in a 1D vertical framework, ~~assuming~~ in which the erosion model is only forced by the meteorological variables with no further interactions between the surface and the atmosphere. We assume that snow re-mobilized from the surface by wind is entirely exported ~~by horizontal transport~~ off the glacier boundaries, which is justified by the local topography, with steep slopes around the glacier ~~,~~ especially toward the east (westerly predominant winds). Due to its one-dimensional, offline nature, our analytical erosion model does not account for horizontal advection of airborne snow from upstream areas, and interactions of airborne snow particles with the atmosphere are neglected. Following Amory et al. (2021), fresh snow is assumed to be deposited with a density ρ of 300 kg m^{-3}, the erosion rate is parameterized as a function of surface snow density ~~only~~ and wind speed, and erosion is not allowed to occur when $\rho \geq 450$ kg m^{-3} or when the air temperature exceeds the freezing point. In this approach the snowpack is described with a 3-layer model, representing a range of ρ values from fresh snow (top layer; $\rho = 300$ kg m^{-3}), erodible aging snow (intermediate layer; 300 kg m^{-3} $< \rho <$ 450 kg m^{-3}) and non-erodible firn (bottom layer; $\rho \geq 450$ kg m^{-3}). This ~~discretization limits the eroded snow mass to the available erodible mass budget and allows accumulation in the firn~~ ensures that the upper limit for the erosion rate is set to the mass content of the two first, erodible layers, and allows dense snow to be permanently added to the snowpack. Snow densification of the top layer is parameterized following a linear densification rate as implemented in MAR, and is considered to occur under the action of erosion only. Note that our model does not resolve the surface energy balance and other mass balance processes (sublimation and melt), and inherently ignores the related snow metamorphism. The snowpack is initialized as a single non-erodible firn layer. The model is described in more details in Appendix A. The meteorological inputs (precipitation, wind speed, air temperature and surface pressure) required to drive the parametrization of wind erosion are directly taken from Potocki et al. (2022), and cover the period 1950-2019 as they originate from ERA5 downscaled data (Hersbach et al., 2020). ~~We use their uncorrected precipitation rates~~ However, instead of using artificially reduced precipitation (averaging at ~~191~~ 66.9 mm a^{-1}) ~~,~~ ~~as the tuned estimates~~ to implicitly account for wind erosion that is missing in Potocki et al. (2022), we prescribe uncorrected precipitation rates (averaging at ~~66.9~~ 191 mm a^{-1}) ~~aimed at correcting for missing wind erosionin Potocki et al. (2022)~~ as we intend to explicitly model wind erosion.

The dominant meteorological conditions at South Col Glacier were previously described (Matthews et al., 2020; Potocki et al., 2022). We focus on ~~wind and precipitation~~ precipitation and wind, which both have a strong seasonal cycle (Fig. 3a). Most of the precipitation falls during the monsoon (June, July, August and September; JJAS). In ~~general,~~ winter (December, January, February; DJF), the winds are extremely strong, with mean daily values approaching 20 m s^{-1} ~~in winter~~ when the westerlies hit the topography (Maussion et al., 2014). During monsoon, the winds progressively decrease, from a daily mean of around 10 m s^{-1} in early June, to 2.5 m s^{-1} in the core of the monsoon season (July and August). After ~~mid September~~ mid-September, the wind speed increases very sharply, marking the end of monsoon (Khadka et al., 2021). As a consequence, the precipitation falling before June is not deposited, and the ~~deposition~~ accumulation efficiency (ratio of daily ~~deposition~~ accumulation over precipitation, defined only when precipitation is non-zero) is close to zero (Fig. 3b). During the course of the monsoon, ~~the deposition efficiency gradually increases, and~~ a large proportion of ~~falling snow~~ deposited precipitation is not eroded, and the accumulation efficiency gradually increases. The cumulative ~~deposition~~ accumulation reaches a maximum in ~~mid September~~ mid-September and ultimately decreases in October, when winds strengthen again, meaning that erosion becomes larger than precipitation, thus leading to a negative ~~deposition~~ accumulation efficiency (Fig. 3b). At that time of the year, in our model, the snow reaches the density of 450 kg m^{-3}, which does not allow any additional erosion.

Over the period ~~1950-2020~~ 1950-2019, the annual uncorrected precipitation ranges from 147 to 259 mm w.e. ~~(mean value 191 mm w.e.)~~, and only 0 to 51 % (mean value 25 %) of the precipitation is deposited, ranging from 0 to 97 mm w.e. (mean value 48 mm w.e.), the rest being eroded by wind. The interannual variability of the ~~deposition~~ accumulation efficiency is high, and the model results are very sensitive to the wind speed (Figs. 3c and d). With a wind speed increased by 30 to 40 %, the annual ~~deposition~~ accumulation is almost reduced to zero (Fig. 3d). Conversely, if the wind speed is 40 % lower, the mean annual ~~deposition~~ accumulation is about 120 mm w.e., which is 63 % of the mean annual precipitation. The results are also very sensitive to the total amount of precipitation, with an increase of 40 % in precipitation corresponding to an increase in the ~~deposition~~ accumulation of 80 % (Fig. 3d).

The ~~model of wind erosion is a simple model that~~ wind erosion model is simple and has large limitations. It takes into account only wind erosion and time-dependent densification of snow, which ~~acts as a negative feedback on~~ regulates erosion. Despite these limitations, the results are in good qualitative agreement with the VENμS images. For instance, the pre-monsoon and early monsoon (MAM) ~~snowfalls disappear~~ snow on South Col Glacier disappears systematically both in the model and images. Then, the images show that the glacier is covered by snow during the core of the monsoon (August), which is when the model finds the highest ~~deposition~~ accumulation efficiency (Fig. 3b). This pattern is conserved when testing the model sensitivity to the wind and precipitation input (Fig. A6). However, the images show erosion, or sublimation, during winter (Fig. A3). This is not ~~predicted~~ reproduced in the model, because ~~the snow reaches a density~~ snow density reaches the erosion limit of 450 kg m^{-3} ~~that is the maximum~~ imposed in the model~~, preventing further erosion. It is noteworthy that sublimation accounts for 100-400 mm w.e. a^{-1} (Potocki et al., 2022), which is larger than the mean annual deposition simulated within the range of precipitation and wind values tested here.~~.

From the analyses of the satellite images and the modeling of wind erosion, we conclude that large parts of the fallen snow are likely eroded or re-mobilized after deposition. Our findings have two main implications. First, we suggest that the South Col

Glacier is entirely covered by snow during large parts of the monsoon season (at least during the whole months of August and

September, in which more than 40 % of the annual melt occurs in Potocki et al. (2022))), strongly limiting the ~~potential for ice~~ amount of incoming short wave radiation, and in turn, limiting surface melt. Second, the fact that the ~~deposition~~ accumulation efficiency is not constant in time, together with the ~~high magnitude of snow erosion, imply that~~ low to negative values of the accumulation efficiency at the end of the monsoon, suggest that (1) the temporal variability of accumulation cannot be properly resolved by reducing precipitation by a constant factor over time, and that (2) wind erosion is a major ~~ablation process, that is not constant in time~~snow ablation process in this area. As a consequence, using "net precipitation" (defined as precipitation after removal of snow by wind erosion in Potocki et al. (2022)) artificially balances the surface mass losses of a snow surface for an arbitrary period. ~~Indeed, the snow that falls during monsoon would have a longer residence time compared to snow which fell outside the monsoon, and would thus integrate the surface energy balance over a much longer period. As a consequence, the~~, and thus the net precipitation rates estimated in Potocki et al. (2022) are likely affected by very large uncertainties.

~~From the wind erosion model, we demonstrate that wind erosion is an important surface mass balance component. However, our model is intrinsically limited because it does not consider the other mass balance processes, such as melt and sublimation.~~ Despite the availability of VENμS images, we cannot determine precisely the temporal share of ice exposed or snow covered conditions for South Col Glacier. We therefore investigate the ablation processes by modeling the glacier mass balance over icy surfaces to consider a worst-case scenario that maximizes ablation (relative to a snow covered scenario).

3.3 The challenge of modeling ~~the~~ surface mass balance

Modeling the changes of ice or snow masses in response to atmospheric forcing is a complex task which involves resolving heat transport and conservation, with concurrent phase changes ~~(e.g., Tubini et al., 2021).~~ (e.g., Anderson, 1976). There are many existing models in the literature which tackle the problem of coupling incoming energy fluxes with subsurface processes. Recent studies show the importance of this coupling to accurately model melt in the firn zone (e.g., Covi et al., 2022; Mattea et al., 2021; MacDone . To model the surface mass balance of the South Col Glacier, Potocki et al. (2022) relied on the COSIPY model (Sauter et al., 2020). They notably found that, in the case of ~~a yearly snow free~~ an all-year snow free glacier surface, the COSIPY model predicts a substantial 1508 mm w.e. a^{-1} of melt on average for the simulation period ~~1950-2020~~1950-2019. The goal of this section is to assess the robustness of this large modeled annual melt. For this purpose, we performed similar mass balance simulations of an ice surface, with different ~~models.~~model configurations. The purpose of the numerical simulations that we perform in this section is not to produce realistic estimates of the surface mass balance prevailing at South Col Glacier, but to show that various acceptable choices in the numerical treatment of the surface energy balance in COSIPY produce very different results in terms of melt.

We ~~compared three different models~~ compare two different model configurations forced with the same meteorological inputs, taken from Potocki et al. (2022), to simulate the ice ablation for the year 2019 (arbitrarily chosen). ~~First, we~~Note that simulations are performed over only one year as the aim is to investigate the fundamental potential of large melt rather than

mimic the entire long term melt evolution. For that, we first use the standard version of COSIPY run with an hourly time-step, as in Potocki et al. (2022). This simulation is named hereafter COSIPY_P22. We then used a slightly modified version of COSIPY with (i) a one minute time-step and (ii) a modified computation of the heat conduction flux between the surface and the ice below, that is abusively referred to as the ground heat flux in COSIPY (Sauter et al., 2020) and in Potocki et al. (2022). Indeed, in the default COSIPY settings used in Potocki et al. (2022), the heat conduction flux is computed by considering the temperature gradient on the first 10 cm of the ice column. However, physically this heat conduction flux is driven by the temperature gradient right under the surface (Sauter et al., 2020). We thus modify the COSIPY source code to compute the temperature gradient as close as possible to the surface. Specifically, we use the temperature values at the surface and at the node below (usually at 1 cm depth), in order to compute the temperature gradient in the vicinity of the surface. This simulation is named hereafter COSIPY_grad. In order to maintain an icy surface in COSIPY_grad, we set the precipitation to zero, thus maintaining albedo at its minimum value and likely enhancing melt. COSIPY_grad simulation is initialized with the thermal state predicted by a COSIPY simulation similar to COSIPY_P22, that ran from 2010-01-01 to 2019-01-01.

COSIPY_P22 predicts a significant amount of melt (1368 mm w.e. for the year 2019), while COSIPY_grad only predicts 15 mm w.e. a^{-1} (Fig. 4). This large difference cannot be accounted for by differences in the radiative or turbulent fluxes, as they are similar for both simulations (Fig. A4). In particular, the daily sublimation rate is very close for both simulations with a cumulative sublimation of 453 and 482 mm w.e. simulated by COSIPY_P22 and COSIPY_grad, respectively, for the year 2019. Furthermore, in both simulations, the surface reaches the melting point during daytime in the monsoon period (Fig. 4), but only COSIPY_P22 predicts a large amount of melt. The simulated surface temperatures are very close, when comparing the hourly averages, with COSIPY_grad being slightly warmer than COSIPY_P22 (RMSE = 2.2 K, mean difference = 0.1 K). However, the daily maxima of COSIPY_P22 are on average 2.1 K higher than COSIPY_grad (Fig. 4).

As both simulations predict surface temperature reaching melting temperature and similar surface fluxes, the discrepancies between their predicted melt can likely be explained by differences in the representation of energy transport. In both COSIPY versions the surface temperature is computed by searching for the temperature that equilibrates the energy fluxes at the surface,

~~further~~. If the equilibrium temperature is above the melting point, the surface temperature is capped at the melting temperature and the excess energy is used for melting the surface. The computation of this equilibrium temperature requires to compute the amount of energy transported by conduction from the surface into the ice column, the so-called ground heat flux in Sauter et al. (2020) and Potocki et al. (2022), and actually representing the subsurface heat conduction flux. As explained above, in the standard COSIPY version this subsurface heat conduction flux is estimated using the first 10 cm of the ice column, and is therefore potentially not representative of the strong temperature gradient that can be present in the direct vicinity (i.e. the first centimeters) of the surface. This can lead to ~~a poor estimate~~ an underestimation of the subsurface heat conduction flux, affecting the amount of energy accumulated at the surface and, in this case, favoring melt. This phenomenon is further exacerbated by the use of an hourly time-step~~and~~, the decoupling of the energy absorption and of the internal heat diffusion processes in COSIPY: energy is accumulated during a full hour before it can be removed by internal diffusion, leading to temperature and melt overshoots. The reduction of the time-step to a minute in COSIPY_P22 reduces the predicted melt by about 30 % (not shown here). We note that the simulation at one hour time-step and a temperature gradient calculated very close to the surface ~~is unrealistic as it results in a~~ leads to unrealistically high mean annual subsurface ~~flux of~~ heat flux (i.e. 600 W m^{-2} ~~. In comparison, in COSIPY_grad the computation of the subsurface conduction heat flux is performed as close as possible~~ to compare to the annual mean incoming shortwave below 300 W m^{-2} for the same period). The calculation of the temperature gradient close to the surface~~. This~~, in combination with a smaller time step, allows the model to efficiently evacuate energy from the surface, hindering melting. As seen in Fig. A5, the COSIPY_grad simulation predicts much higher subsurface heat conduction fluxes during the monsoon period, strongly limiting the surface melt.

~~Finally, in Crocus the surface temperature is computed by considering a finite thickness for the first layer as opposed to COSIPY, which is a skin temperature model (e.g., Covi et al., 2022). Consequently Crocus does not require the computation of the surface temperature that equilibrates the surface energy fluxes, and thus does not need to approximate the subsurface heat conduction flux. Furthermore, in Crocus the absorption and conduction of energy are performed simultaneously, making it less likely to locally accumulate enough heat for melting.~~

This numerical experiment demonstrates that the structure and ~~configuration~~ physical implementation of a model can strongly affect the way the energy is spatially allocated and transported, leading to large variations in predicted melt despite solving, in principle, the same physical processes. Notably, the COSIPY_grad ~~and CROCUS_ice simulations highlight~~ simulation highlights that physically consistent modeling configurations can lead to little ~~or no~~ melt when considering the energy budget of an ice surface in the conditions of South Col Glacier. However, we raise some awareness about the parametrization choices made for the simulation, such as for instance the albedo, that increase the model uncertainty. Indeed, the blue ice of South Col Glacier might have a larger albedo than 0.4, as it is observed for Antarctic blue ice that has an albedo of 0.5 to 0.6 (e.g., Smedley et al., 2020). A higher ice albedo would dramatically reduce the melt totals, as suggested by the sensitivity tests of Potocki et al. (2022) and Machguth and Mattea (2022). In view of ~~this~~ the large modeling uncertainty, and without measurements, it is therefore not possible to ~~definitely~~ definitively conclude on the amount of surface melting when ice is exposed on South Col Glacier (i.e. when snow-free conditions are observed in June and potentially July) solely from a modeling point of view. ~~However, the very large annual melt totals in COSIPY_P22 appear, at least, very questionable. This is reinforced~~

by the little evidence for large amounts of melt happening at South Col Glacier. For instance, there are no large supraglacial stream features visible in the aerial photographs or satellite imagery, even though they would be expected to develop when 1.5 m w.e. of iceis melted every year. Similarly, in the photographs of the glacier surroundings, there is no evidence of runoff, such as stones being embedded into in re-frozen water , or crevasses being filled by re-frozen ice , all of which are usually observed when melt occurs on cold glaciers. Yet, these qualitative observations cannot be used as model evaluation. Additionally, even though there would be some surface melt on this glacier, it is likely that a large amount of this meltwater would refreeze at the surface in case of the presence of snow or firn, or would form superimposed ice. While COSIPY accounts for refreezing in snow, it considers water originating from an ice surface as runoff, limiting its applicability in such a cold context. We thus highlight here that snow and ice energy balance models are developed and tested in specific conditions, and might not be applied directly to other conditions, such as the very COSIPY does not seem to be suitable to model mass balance in the specific conditions of South Col glacier, Glacier without extensive validation.

4 Implications for the interpretations interpretation of the South Col Glacier ice core

In the original interpretation of the South Col Glacier ice core, (Potocki et al., 2022) Potocki et al. (2022) dated the top 10–69 cm of the core and found an age of 1966 $\pm$ 179 years. Based on a layer counting estimate of annual accumulation of 27 mm w.e. a^{-1}, they concluded that ~55 m of ice was missing and has were missing and have been removed. Relying on surface mass balance modeling with COSIPY, they estimated contemporary thinning local mass balance rates approaching 2 m a^{-1}, and thus dated the initiation of thinning in the 1990s, leading to a cumulative mass loss of ~55 m by 2019.

. The interpretation of Potocki et al. (2022) relies on two assumptions: (i) a continuous and stable accumulation of $\sim$ 27 mm w.e. a^{-1} for a 2000 year period and (ii) the absence of ice flow and ice emergence that would transport old ice from the accumulation zone to the surface of the ablation zone(e.g. Fig. 1, Jouvet et al., 2020).

Regarding (i), given the small value for accumulation, and the magnitude and variability in wind erosion, it seems difficult to accept that accumulation is stable and continuous. Moreover, the accumulation is estimated based on 10 m of ice, which consequently corresponds would consequently correspond to an approximate duration of only 330 years. The assumption that similar surface mass balance conditions persisted for up to the past 2000 years is therefore based on a large extrapolation. If the accumulation was not continuous, i.e. if there are some missing years in the core records, then the 1966 $\pm$ 179 year old ice exposed near to the surface would not imply 55 m of missing ice. More precise dating of the deeper sections of the South Col Glacier ice core could help resolve the question of continuity of accumulation. Note that our present study focuses on the period 1984-2017 (or 1956-2022; Machguth and Mattea, 2022) where no thinning is observed, but we cannot exclude any thickening and/or thinning episodes anterior to this period, potentially explaining why Potocki et al. (2022) observed ice as old as 1966 years at the surface of their ice core.

350 Regarding (ii), Potocki et al. (2022) neglected ice flow, and thus did not distinguish surface mass balance and elevation/thickness change. However, South Col Glacier is flowing at an unknown velocity as evidenced by the presence of a bergschrund, large crevasses and primary stratification visible on the Pléiades ~~ortho image~~ orthoimage (Fig. **??**1c). Given that the ice core has a density of ~~0.89~~ 890 kg m^{-3}, and that no firn is mentioned in Potocki et al. (2022), we ~~suggest interpret the core was drilled in the ablation area of South Col Glacier. Based on the drilling location, the glacier topography and the presence of exposed~~

355 ~~ice visible on Pléiades ortho image, we delineate a minimum extent of the ablation area of South Col Glacier (Fig. **??**). Our observations from DEM difference (Section 2) show that the elevation change of South Col Glacier is close to zero for the period 1984-2017 implying that ablation is compensated by the ice flux (Φ in m^3 a^{-1}) coming from the accumulation area~~ are wondering whether the core could have been drilled in an area of the glacier where ablation conditions frequently prevail. As a consequence, the divergence of ice flux would be negative and ice would emerge, leading to ~~(e.g., Cuffey and Paterson, 2010):~~

360

$$\Phi = L\bar{H}\bar{U} = \dot{b}_{abl}A_{abl}$$

~~where L is the length of the section (L = 670 m here, Fig. **??**), $\bar{H}$ is~~ old ice being exposed at the surface. One possible interpretation, is that avalanches occurring at the foot of Everest's south-east face feed an area of the ~~mean depth along the section (we conservatively assume $\bar{H}$ = 50 m here), $\bar{U}$ is the depth-averaged velocity along the section (in m a^{-1}), $\dot{b}_{abl}$ is the~~

365 ~~area averaged surface mass balance in the ablation area (assumed to be 2 m a^{-1}) and A_{abl} is the area of the ablation area (A_{abl} = 0.14 km^2 here). This back of the envelope calculation leads to a depth-averaged velocity of 8.5 m a^{-1}, which is unrealistically high (for reference, the drilling site is located only 150 m downstream of the bergschrund and the velocity deformation is estimated at 0.2 to 0.7 m a^{-1} for an ice thickness of 50 m and is an order of magnitude smaller for 25 m of ice; see Appendix C)~~ glacier with dense snow that is more difficult to erode, leading to a local excess of mass, and thus actual accumulation. For

370 the rest of the glacier area, erosion and sublimation, that are both controlled by wind, maintain a near-zero balance between accumulation and ablation.

~~Finding~~ Furthermore, finding ice that is as old as 1966 $\pm$ 179 years at the surface suggests that South Col Glacier is flowing very slowly. Given that the ~~core was drilled less than~~ distance between the bergschrung and the drilling site is approximately

375 150 m ~~downstream of the bergschrund, the maximum velocity averaged along the flow line is approximately 7 cm~~ (Fig. A1), ice as old as 1966 $\pm$ 179 years cannot be encountered in the core if the average velocity exceeds 150/1966 = 0.08 m a^{-1}~~, but could be much smaller as we~~. We do not know where ~~the~~ this ice formed along ~~this flowline~~ the flow line, so the horizontal velocity is likely lower than this maximum estimate of 0.08 m a^{-1}. The South Col Glacier is thus likely a ~~very continental type of~~ glacier with small ice fluxes. This would be in good agreement with our modeling of wind erosion and surface mass balance,

380 suggesting arid conditions. A large fraction of precipitation (> 60 %) is ~~not deposited, limiting the incoming precipitation deposition~~ eroded, limiting accumulation. Then sublimation is likely the dominant ablation process, that removes 90 to 450 mm w.e. of snow or ice per year ~~(Potocki et al., 2022)~~ (this study and Potocki et al., 2022), leading to a very ~~small~~ limited mass turnover (i.e. low absolute value of surface mass balance), ~~and therefore~~ in agreement with small ice fluxes (e.g., Cuffey and Paterson, 2010).

385 ~~One alternative process is that avalanches occurring at the foot of Everest south east face feed the accumulation area of the glacier with dense snow that is more difficult to erode, leading to a local excess of mass, and thus actual accumulation. For the rest of the glacier area, deposition and sublimation, that are both controlled by wind, maintain a thin balance between accumulation and ablation.~~

5 Conclusions

390 In our study, we demonstrate on the basis of remote sensing information that no significant elevation change occurred at South Col Glacier between 1984 and 2017. This is in contrast with the ~~postulated strong melt, or thinning, rates~~ strong rates of melt (or thinning) postulated by Potocki et al. (2022), of almost 2 m a^{-1} at the location of the ice core during the recent past~~proposed by Potocki et al. (2022)~~. Our results show that ~~large magnitude of melt is~~ high melt rates are unlikely to happen on South Col Glacier for ~~three~~ two main reasons: i- the glacier is covered by snow during ~~large parts of~~ most of the monsoon season, limit-

395 ing the net incoming shortwave radiation, and ii- the glacier did not thin over the last three decades and the ice core analysis suggests low velocities and thus low mass turnover. Moreover, when the glacier surface consists of exposed ice, ~~the occurrence~~ which is the case where highest melt is expected due to low albedo, the magnitude of melt is highly dependent on modeling choices (i.e. model structure and parameters) for similar meteorological inputs, and the COSIPY model structure might not be well suited for this particular application~~, and iii- first order estimates of ice fluxes do not allow for a large amplitude of mass

400 turnover~~.

The surface mass balance processes happening in the extreme meteorological context of South Col Glacier are complex, and our study does not reach any definitive conclusion about the relative importance of each of these processes. The lack of direct observations hampers our ability to decipher the dominant glaciological processes, and thus to model the glacier recent and

405 future evolution in a realistic way. Specifically, stake measurements would be needed to measure the surface mass balance and surface velocity in a direct way, ground penetrating radar measurements would help constrain the ice thickness, and a number of subsurface temperature, snow-depth, snow transport or turbulent fluxes measurements would help constrain the processes. Without more ~~data constrained~~ observational knowledge, it appears currently ~~impossible~~ very difficult to conclude about the sensitivity of South Col Glacier to climate change, nor to predict its future evolution.

410 *Code and data availability.* The dH map is on a public repository together with the arerial photograph DEM (https://doi.org/10.5281/zenodo.7529761). The Pléiades DEM is available at https://doi.org/10.5281/zenodo.6979691 (Berthier, 2022). License restrictions apply to the Pléiades ortho images, that are available upon request to E.B., pending the signature of license agreement with CNES.

The uncertainty analysis code is available at: https://github.com/rhugonnet/uncertainty_analysis_SCG/blob/main/uncert_SCG_from_Hugonnet2022.ipynb, and based on the Python package xDEM available at: https://github.com/GlacioHack/xdem.

415 VENµS data are available at: https://doi.org/10.5281/zenodo.6685515 (Brun, 2022)

The wind erosion code is available at: https://github.com/antonplanchot/wind-snow-scg (Planchot and Amory, 2022)

Appendix A: Parameterizing wind erosion

The contribution of wind erosion of snow to the local glacier mass balance results from three-dimensional interactions of the atmospheric flow with the surface which thus, in principle, cannot be properly treated with a one-dimensional model. Although the erosion process, which describes the removal of snow from the surface by wind, may be expressed in a one-dimensional vertical framework, the net export of snow by horizontal transport, however, needs resolving in the horizontal dimensions by definition. Due to the relatively small dimensions of the glacier (0.2 km^2) and its complex topographical surroundings, capturing the erosion process over this full range of spatial scales requires an eddy-resolving, three-dimensional model with a very fine, meter-scale horizontal resolution and appropriate lateral boundary fluxes. This approach would also require a very large amount of computational resources and is thus not suited for climatological time scales. As a much more computationally efficient alternative, we used a simplified approach to parameterize wind erosion of snow as a one-dimensional vertical model.

Our parameterization is inspired from the erosion scheme of the regional climate model MAR (Gallée et al., 2001; Amory et al., 2021) and assumes a complete export of eroded snow outside of the glacier boundaries by horizontal wind transport. This assumption is crude but has some theoretical support. Due to the geometry and the NE-SW orientation of the South Col Glacier (Fig. 1), westerlies are the dominant and strongest local winds (Fig. A7) as a result of local topographical channeling. They may thus mostly be responsible for snow erosion and export off the eastern side of the glacier. An illustration of this process is the striking expansion of blue ice surfaces revealed by analysis of VENμS images during the last quarter of year 2019 (Fig. 2), when strong wind speeds of high erosive potential occur after the monsoon season. Another way to support this assumption is to confirm that a snow model equipped with a parameterization of wind erosion can reproduce this feature.

Wind erosion is usually considered to initiate when the friction velocity, u_* (m s^{-1}), exceeds a threshold value, u_{*t} (m s^{-1}), mostly determined by snow microstructural characteristics at the surface including snow density, grain size and bond number and strength (Schmidt, 1980). In our model, the friction velocity u_* is derived from the 2-m local wind speed forcing U, directly taken from Potocki et al. (2022) and assuming a logarithmic wind profile:

$$u_* = \frac{kU}{\ln(2/z_0)} \tag{A1}$$

where k is the von Kármán constant (0.4) and z_0 the roughness length for momentum set to 10^{-4} m. Following Amory et al. (2021), in the absence of observational characterization of local surface snow characteristics, the threshold friction velocity u_{*t} is expressed as a function of snow surface density only:

$$u_{*t} = u_{*t0} \exp\left(\frac{\rho_{ice}}{\rho_0} - \frac{\rho_{ice}}{\rho_s} \right) \tag{A2}$$

with u_{*t0} the expression for the standard friction velocity (0.211 m s^{-1}), ρ_{ice} the density of ice (920 kg m^{-3}), ρ_0 the density of fresh snow (set to 300 kg m^{-3}) and ρ_s the density of surface snow (kg m^{-3}).

When $u_* > u_{*t}$, the air temperature is below the freezing point and the surface snow density is below 450 kg m^{-3} (see below), the particle ratio in the saltation layer q_{salt} (kg kg^{-1} ; mass of saltating snow particles per unit mass of atmosphere) is

computed as a function of the excess of shear stress responsible for removal of snow particles from the surface:

$$q_{salt} = \frac{u_*^2 - u_{*t}^2}{gh_{salt}}e_{salt} \tag{A3}$$

where g = 9.81 the gravitational acceleration (m s^{-2}), $h_{salt} = 0.08436u_*^{1.27}$ is the height of the saltation layer (m) and $e_{salt} = \frac{1}{3.25u_*}$ is the saltation efficiency expressed as a dimensionless coefficient inversely proportional to the friction velocity. A surface turbulent flux of snow, referred to as potential erosion E_p (m s^{-1} kg kg^{-1}), is then approximated assuming that it follows a bulk formula:

$$E_p = C_D U(q_{salt} - q_s) \tag{A4}$$

where C_D is a drag coefficient (10^{-3}) similar to that used for sensible and latent heat fluxes, U is the near-surface wind at standard level (10 m) and q_s is the snow particle ratio (kg kg^{-1}) at the same level. Assuming that any re-mobilized snow is quickly removed by horizontal transport, then q_{salt} - $q_s \approx q_{salt}$, and re-expressing U assuming a logarithmic wind profile, E_p ~~writes~~is given by:

$$E_p = C_d q_{salt} \frac{u_*}{k} \ln\left(\frac{10}{z_0}\right) \tag{A5}$$

Equation A3 contains semi-empirical formulations assumed to implicitly account for all the physical processes that contribute the airborne snow mass, including the gravitational settling of snow particles. Equation A5 expresses turbulent vertical exchange between the saltation layer and the overlying atmosphere but not settling. However, the saltation layer contains significant quantities of snow under strong winds (Nemoto and Nishimura, 2004; Huang et al., 2016), in which case turbulence is a dominant contributor over settling which is consequently ignored. We then deduce an expression for the maximum amount of erodible snow ER (kg m^{-2}) during one time step dt (1 h):

$$ER = E_p \rho_{air} dt \tag{A6}$$

where ρ_{air} = P/(RT) is the density of air (kg m^{-3}), P the surface pressure (Pa), R = 287 the specific gas constant (J kg^{-1} K^{-1}) and T the air temperature (K). The effective erosion ER_{eff} (kg m^{-2}) is then taken as the minimum between the maximal erosion ER and the available snow mass for erosion (mass content in the top and intermediate layer) in the snow model. Note that ~~u*t~~ u_{*t} is recomputed for each snow layer. If a layer is completely eroded during a time step, the layer below is also eroded during the same time step. The maximal erosion ER of this layer is then computed taking into account the time spend to erode the upper layer.

In natural environments, wind erosion contributes to the densification of the snow surface due to the combined actions of wind and saltation which break original crystal shapes and favour the formation of smaller, rounded snow grains (Sato et al., 2008), leading to enhanced sintering, more efficient mechanical packing and increased density (Vionnet et al., 2013). Erosion-induced densification, together with the exposure of denser snow or ice layers through erosion, both naturally contribute to reduce the likelihood of additional erosion. In our model, erosion-induced densification is applied to the top snow layer that

has experienced erosion following a linear densification rate from the fresh snow value ρ_0 (assumed to be representative of snow that have been barely altered by post-depositional processes) to the prohibitive density value for snow erosion ρ_{max}:

$$\frac{d\rho_s}{dt} = \frac{\rho_{max} - \rho_0}{\tau_{ER}} \tag{A7}$$

where $\rho_{max} = 450 \text{ kg m}^{-3}$ and τ_{ER} is the characteristic time scale for erosion-induced densification set to 24 h. As our model time step (~~our~~ one hour) is small compared to τ_{ER}, the negative feedback of snow erosion within one time step can be neglected and is only active from one time step to another.

After the densification step, if the snow density exceeds the density criteria of the layer, it is transferred to the next denser layer. When snow is moved from the top layer to the intermediate layer, the density of the intermediate layer is recomputed by weighted average of the former ~~thickness~~ thicknesses of each layers.

Our model is a simplified approach aiming at quantifying the effect of wind erosion on the mass balance of the South Col Glacier. Other ablation processes (melt, sublimation) resulting from the surface energy balance, snow metamorphism processes and snowpack internal changes in snow characteristics which can lead to additional densification are neglected. However, we expect few implications since erosion of a snow layer of density above ρ_{max} of 450 kg m^{-3} is prohibited. Even if some internal model parameters (ρ_0, ρ_{max}, τ_{ER}) have been scaled for Antarctic conditions (Amory et al., 2021), we simply re-used without additional tuning the original configuration of MAR, considering the similarities in the climatological context between Coastal Antarctica and the South Col Glacier (extreme wind speeds and relatively low air temperatures).

The erosion parameterization proposed above is admittedly very approximate. It ignores notably the sublimation of airbone snow (Gallée et al., 2001). However, as we assume a complete export of drifting snow, whether the suspended snow is finally exported in the solid or vapor phase makes no difference. Although other formulations of wind erosion could be devised, a more constrained parameterization could not necessarily be developed without additional measurements or through a coupling with a multidimensional model and/or a multilayer snow model. Our main point here is that, in order to explain the gradual removal of snow and resulting appearance of blue ice areas as revealed from analysis of VENμS images and understand the reasons behind its temporal variability, it is necessary to account for wind erosion.

Appendix B: ~~Crocus Model~~

~~Crocus is a full energy balance, one-dimensional snowpack model, driven by meteorological variables. It simulates a layered snowpack with a Lagrangian representation, each layer being characterised by its thickness, density, temperature, liquid water content and two semi-empirical variables to describe the snow/ice microstructure (i.e. SSA and sphericity).The model solves the heat diffusion equation in the snowpack at a 15 min time step considering the different energy fluxes between the surface and the atmosphere and between the bottom of the snowpack and the soil. Physical processes such as solar radiation absorption, liquid water percolation, snow metamorphism and settlement are also considered by the model. While it was originally developed to simulate seasonal snowpack and to assist in avalanche hazard forecasting over the French mountain ranges (Vionnet et al., 2012), the model can be used on icy surfaces, considering an ice layer as a specific snow layer with~~

a density of 917 kg m^{-3} (Gerbaux et al., 2005; Lejeune et al., 2007; Dumont et al., 2012; Réveillet et al., 2018). However, to our knowledge, the model has never been applied to simulate cold glacier mass balance and a careful evaluation would be necessary to further apply Crocus in such context.

515 Crocus model is forced using the same hourly meteorological forcing described in Potocki et al. (2022). The 'ice simulation' is performed without considering the precipitation (to ensure simulating icy surface mass balance only). Initialisation of the ice thickness and thermal profile is initialized with the state predicted by a COSIPY simulation that ran from 2010-01-01 to 2019-01-01 from Potocki et al. (2022). Model parameterization (i.e. ice albedo, ice roughness values, atmosphere stability correction) is done following the study of Potocki et al. (2022). More details, data to reproduce the simulations and simulation

520 outputs are found at: https://doi.org/10.5281/zenodo.7006744

Appendix B: **Estimating the surface velocity due to ice deformation**

The surface velocity (u_s in m s^{-1}) of a glacier can be approximated as (Cuffey and Paterson, 2010):

$$u_s = u_b + \frac{A}{n+1}\tau_b^n H$$

where u_b (in m s^{-1}) is the basal velocity, assumed to be zero for cold glaciers, A (in s^{-1} Pa^{-3}) is the creep parameter , n is

525 the exponent of Glen's flow law, H (in m) in the ice thickness (Cuffey and Paterson, 2010). τ_b (in Pa) is the basal shear stress, expressed as:

$$\tau_b = \rho_{ice}gH\alpha$$

Where $\rho_{ice} = 0.9 \times 10^3$ kg m^{-3} is the ice density, $g = 9.81$ m s^{-2} is the gravitational acceleration, and $\alpha = 0.36$, is the slope (corresponding to 20 degrees). We take $n = 3$, and the values recommended for A (Table 3.4, pp 75 in Cuffey and Paterson, 2010)

530 . We assume 1 year = 3.16 $\times 10^7$ s. The results are shown in Table **??**.

Surface velocity (in m a^{-1}) for different ice temperatures and ice thicknesses T ($^{\circ}$C) / Thickness (m) 5 10 25 50 1000 7.6$\times 10^{-4}$ 1.2$\times 10^{-2}$ 4.8$\times 10^{-1}$ 7.6$\times 10^{0}$ 1.2$\times 10^{2}$ -5 3.0$\times 10^{-4}$ 4.7$\times 10^{-3}$ 1.8$\times 10^{-1}$ 3.0$\times 10^{0}$ 4.7$\times 10^{1}$ -10 1.1$\times 10^{-4}$ 1.8$\times 10^{-3}$ 6.9$\times 10^{-2}$ 1.1$\times 10^{0}$ 1.8$\times 10^{1}$ -15 6.7$\times 10^{-5}$ 1.1$\times 10^{-3}$ 4.2$\times 10^{-2}$ 6.7$\times 10^{-1}$ 1.1$\times 10^{1}$ -20 3.8$\times 10^{-5}$ 6.1$\times 10^{-4}$ 2.4$\times 10^{-2}$ 3.8$\times 10^{-1}$ 6.1$\times 10^{0}$ -25 2.2$\times 10^{-5}$ 3.5$\times 10^{-4}$ 1.4$\times 10^{-2}$ 2.2$\times 10^{-1}$ 3.5$\times 10^{0}$

535 *Author contributions.* FB, MR and CA designed the study. OK, EB, FB, AD and RH generated the DEMs and analyzed DEM differences, MR, KF, JB, FB and MD analyzed the results of the surface mass balance models, CA and AP developed the wind erosion model and analyzed the results. SL analyzed Sentinel-1 back-scatter series (not shown in the brief communication). FB led the writing and all the authors contributed to it.

Competing interests. Some authors are members of the editorial board of The Cryosphere. The peer-review process was guided by an

540   independent editor, and the authors have also no other competing interests to declare.

Acknowledgements. CNRM/CEN is part of Labex OSUG@2020. Marie Dumont, Julien Brondex and Kevin Fourteau have received funding from the European Research Council (ERC) under the European Union's Horizon 2020 research and innovation program (IVORI (grant no. 949516)). E.B. acknowledges support from the French Space Agency (CNES). We ~~thank Evan Miles and Vincent Favier for insightful discussions and comments~~ acknowledge support from the ANR for the iFROG project (ANR-21-CE01-0012).

References

Agosta, C., Amory, C., Kittel, C., Orsi, A., Favier, V., Gallée, H., van den Broeke, M. R., Lenaerts, J. T. M., van Wessem, J. M., van de Berg, W. J., and Fettweis, X.: Estimation of the Antarctic surface mass balance using the regional climate model MAR (1979–2015) and identification of dominant processes, The Cryosphere, 13, 281–296, https://doi.org/10.5194/tc-13-281-2019, 2019.

Amory, C., Kittel, C., Le Toumelin, L., Agosta, C., Delhasse, A., Favier, V., and Fettweis, X.: Performance of MAR (v3.11) in simulating the drifting-snow climate and surface mass balance of Adélie Land, East Antarctica, Geoscientific Model Development, 14, 3487–3510, https://doi.org/10.5194/gmd-14-3487-2021, 2021.

Anderson, E. A.: A point energy and mass balance model of a snow cover, https://repository.library.noaa.gov/view/noaa/6392, 1976.

Berthier, E.: Pléiades DEM of 23 March 2017 - Khumbu region, Nepal, https://doi.org/10.5281/zenodo.6979691, 2022.

Berthier, E., Vincent, C., Magnússon, E., Gunnlaugsson, A., Pitte, P., Le Meur, E., Masiokas, M., Ruiz, L., Pálsson, F., Belart, J. M. C., and Wagnon, P.: Glacier topography and elevation changes derived from Pléiades sub-meter stereo images, The Cryosphere, 8, 2275–2291, https://doi.org/10.5194/tc-8-2275-2014, 2014.

Bessin, Z., Dedieu, J.-P., Arnaud, Y., Wagnon, P., Brun, F., Esteves, M., Perry, B., and Matthews, T.: Processing of VENμS Images of High Mountains: A Case Study for Cryospheric and Hydro-Climatic Applications in the Everest Region (Nepal), Remote Sensing, 14, 1098, https://doi.org/10.3390/rs14051098, 2022.

Beyer, R. A., Alexandrov, O., and McMichael, S.: The Ames Stereo Pipeline: NASA's Open Source Software for Deriving and Processing Terrain Data, Earth and Space Science, 5, 537–548, https://onlinelibrary.wiley.com/doi/abs/10.1029/2018EA000409, 2018.

Brun, F.: Natural color composites of VENμS images over South Col Glacier, https://doi.org/10.5281/zenodo.6685515, type: dataset, 2022.

Covi, F., Hock, R., and Reijmer, C. H.: Challenges in modeling the energy balance and melt in the percolation zone of the Greenland ice sheet, Journal of Glaciology, pp. 1–15, https://doi.org/10.1017/jog.2022.54, 2022.

Cuffey, K. M. and Paterson, W. S. B.: The physics of glaciers, Academic Press, 2010.

Dick, A., Raynaud, J.-L., Rolland, A., Pelou, S., Coustance, S., Dedieu, G., Hagolle, O., Burochin, J.-P., Binet, R., and Moreau, A.: VENμS: Mission Characteristics, Final Evaluation of the First Phase and Data Production, Remote Sensing, 14, 3281, https://doi.org/10.3390/rs14143281, 2022.

Dumont, M., Durand, Y., Arnaud, Y., and Six, D.: Variational assimilation of albedo in a snowpack model and reconstruction of the spatial mass-balance distribution of an alpine glacier, Journal of Glaciology, 58, 151–164, https://doi.org/10.3189/2012JoG11J163, 2012.

Fischer, M., Huss, M., and Hoelzle, M.: Surface elevation and mass changes of all Swiss glaciers 1980–2010, The Cryosphere, 9, 525–540, https://doi.org/10.5194/tc-9-525-2015, 2015.

Gallée, H., Guyomarc'h, G., and Brun, E.: Impact Of Snow Drift On The Antarctic Ice Sheet Surface Mass Balance: Possible Sensitivity To Snow-Surface Properties, Boundary-Layer Meteorology, 99, 1–19, https://doi.org/10.1023/A:1018776422809, 2001.

Gerbaux, M., Genthon, C., Etchevers, P., Vincent, C., and Dedieu, J.: Surface mass balance of glaciers in the French Alps: distributed modeling and sensitivity to climate change, Journal of Glaciology, 51, 561–572, 2005.

Hersbach, H., Bell, B., Berrisford, P., Hirahara, S., Horányi, A., Muñoz-Sabater, J., Nicolas, J., Peubey, C., Radu, R., and Schepers, D.: The ERA5 global reanalysis, Quarterly Journal of the Royal Meteorological Society, 146, 1999–2049, https://doi.org/10.1002/qj.3803, 2020.

Hirschmuller, H.: Stereo Processing by Semiglobal Matching and Mutual Information, IEEE Transactions on Pattern Analysis and Machine Intelligence, 30, 328–341, https://doi.org/10.1109/TPAMI.2007.1166, 2008.

Huang, N., Dai, X., and Zhang, J.: The impacts of moisture transport on drifting snow sublimation in the saltation layer, Atmospheric Chemistry and Physics, 16, 7,523–7,529, https://doi.org/10.5194/acp-16-7523-2016, 2016.

Hugonnet, R., McNabb, R., Berthier, E., Menounos, B., Nuth, C., Girod, L., Farinotti, D., Huss, M., Dussaillant, I., Brun, F., and Kääb, A.: Accelerated global glacier mass loss in the early twenty-first century, Nature, 592, 726–731, https://doi.org/10.1038/s41586-021-03436-z, 2021.

Hugonnet, R., Brun, F., Berthier, E., Dehecq, A., Mannerfelt, E. S., Eckert, N., and Farinotti, D.: Uncertainty Analysis of Digital Elevation Models by Spatial Inference From Stable Terrain, IEEE Journal of Selected Topics in Applied Earth Observations and Remote Sensing, 15, 6456–6472, 2022.

IPCC: Climate Change 2021: The Physical Science Basis. Contribution of Working Group I to the Sixth Assessment Report of the Intergovernmental Panel on Climate Change, vol. In Press, Cambridge University Press, Cambridge, United Kingdom and New York, NY, USA, https://doi.org/10.1017/9781009157896, 2021.

Jouvet, G., Röllin, S., Sahli, H., Corcho, J., Gnägi, L., Compagno, L., Sidler, D., Schwikowski, M., Bauder, A., and Funk, M.: Mapping the age of ice of Gauligletscher combining surface radionuclide contamination and ice flow modeling, The Cryosphere, 14, 4233–4251, https://doi.org/10.5194/tc-14-4233-2020, 2020.

Khadka, A., Matthews, T., Perry, L. B., Koch, I., Wagnon, P., Shrestha, D., Sherpa, T. C., Aryal, D., Tait, A., Sherpa, T. G., Tuladhar, S., Baidya, S. K., Elvin, S., Elmore, A. C., Gajurel, A., and Mayewski, P. A.: Weather on Mount Everest during the 2019 summer monsoon, Weather, 76, 205–207, https://doi.org/10.1002/wea.3931, 2021.

King, O., Bhattacharya, A., Ghuffar, S., Tait, A., Guilford, S., Elmore, A. C., and Bolch, T.: Six Decades of Glacier Mass Changes around Mt. Everest Are Revealed by Historical and Contemporary Images, One Earth, 3, 608–620, https://doi.org/https://doi.org/10.1016/j.oneear.2020.10.019, 2020.

Lejeune, Y., Bouilloud, L., Etchevers, P., Wagnon, P., Chevallier, P., Sicart, J.-E., Martin, E., and Habets, F.: Melting of snow cover in a tropical mountain environment in Bolivia: Processes and modeling, Journal of Hydrometeorology, 8, 922–937, 2007.

Litt, M., Shea, J., Wagnon, P., Steiner, J., Koch, I., Stigter, E., and Immerzeel, W.: Glacier ablation and temperature indexed melt models in the Nepalese Himalaya, Scientific Reports, 9, 5264, https://doi.org/10.1038/s41598-019-41657-5, 2019.

MacDonell, S., Kinnard, C., Mölg, T., Nicholson, L., and Abermann, J.: Meteorological drivers of ablation processes on a cold glacier in the semi-arid Andes of Chile, The Cryosphere, 7, 1513–1526, https://doi.org/10.5194/tc-7-1513-2013, 2013.

Machguth, H. and Mattea, E.: H. Machguth and E. Mattea: Review of tc-2022-166, https://doi.org/10.5194/tc-2022-166-rc4, 2022.

Mattea, E., Machguth, H., Kronenberg, M., van Pelt, W., Bassi, M., and Hoelzle, M.: Firn changes at Colle Gnifetti revealed with a high-resolution process-based physical model approach, The Cryosphere, 15, 3181–3205, https://doi.org/10.5194/tc-15-3181-2021, 2021.

Matthews, T., Perry, L. B., Koch, I., Aryal, D., Khadka, A., Shrestha, D., Abernathy, K., Elmore, A. C., Seimon, A., Tait, A., Elvin, S., Tuladhar, S., Baidya, S. K., Potocki, M., Birkel, S. D., Kang, S., Sherpa, T. C., Gajurel, A., and Mayewski, P. A.: Going to Extremes: Installing the World's Highest Weather Stations on Mount Everest, Bulletin of the American Meteorological Society, 101, E1870–E1890, https://doi.org/10.1175/BAMS-D-19-0198.1, 2020.

Maussion, F., Scherer, D., Mölg, T., Collier, E., Curio, J., and Finkelnburg, R.: Precipitation Seasonality and Variability over the Tibetan Plateau as Resolved by the High Asia Reanalysis, Journal of Climate, 27, 1910–1927, https://doi.org/10.1175/JCLI-D-13-00282.1, 2014.

Nemoto, M. and Nishimura, K.: Numerical simulation of snow saltation and suspension in a turbulent boundary layer, J. Geophys. Res., 109, https://doi.org/10.1029/2004JD004657, 2004.

Nuth, C. and Kääb, A.: Co-registration and bias corrections of satellite elevation data sets for quantifying glacier thickness change, The Cryosphere, 5, 271–290, https://doi.org/10.5194/tc-5-271-2011, 2011.

620 Planchot, A. and Amory, C.: Three layer wind erosion model for South Col Glacier, https://github.com/antonplanchot/wind-snow-scg, type: code, 2022.

Potocki, M., Mayewski, P. A., Matthews, T., Perry, L. B., Schwikowski, M., Tait, A. M., Korotkikh, E., Clifford, H., Kang, S., Sherpa, T. C., Singh, P. K., Koch, I., and Birkel, S.: Mt. Everest's highest glacier is a sentinel for accelerating ice loss, npj Climate and Atmospheric Science, 5, 7, https://doi.org/10.1038/s41612-022-00230-0, 2022.

625 Rolstad, C., Haug, T., and Denby, B.: Spatially integrated geodetic glacier mass balance and its uncertainty based on geostatistical analysis: application to the western Svartisen ice cap, Norway, Journal of Glaciology, 55, 666–680, https://doi.org/10.3189/002214309789470950, 2009.

Réveillet, M., Six, D., Vincent, C., Rabatel, A., Dumont, M., Lafaysse, M., Morin, S., Vionnet, V., and Litt, M.: Relative performance of empirical and physical models in assessing the seasonal and annual glacier surface mass balance of Saint-Sorlin Glacier (French Alps),
630 The Cryosphere, 12, 1367–1386, https://doi.org/10.5194/tc-12-1367-2018, 2018.

Sakai, A.: Brief communication: Updated GAMDAM glacier inventory over high-mountain Asia, The Cryosphere, 13, 2043–2049, https://doi.org/10.5194/tc-13-2043-2019, 2019.

Sato, T., Kosugi, K., S., M., and M., N.: Wind speed dependences of fracture and accumulation of snowflakes on snow surface, Cold Regions Science and Technology, 51, 229–239, https://doi.org/10.1016/j.coldregions.2007.05.004, 2008.

635 Sauter, T., Arndt, A., and Schneider, C.: COSIPY v1.3 – an open-source coupled snowpack and ice surface energy and mass balance model, Geoscientific Model Development, 13, 5645–5662, https://doi.org/10.5194/gmd-13-5645-2020, 2020.

Schmidt, R. A.: Threshold wind-speeds and elastic impact in snow transport, Journal of Glaciology, 26, 453–467, https://doi.org/10.3189/S0022143000010972, 1980.

Shean, D. E., Alexandrov, O., Moratto, Z. M., Smith, B. E., Joughin, I. R., Porter, C., and Morin, P.: An automated, open-source pipeline for
640 mass production of digital elevation models (DEMs) from very-high-resolution commercial stereo satellite imagery, {ISPRS} Journal of Photogrammetry and Remote Sensing, 116, 101 – 117, https://doi.org/http://dx.doi.org/10.1016/j.isprsjprs.2016.03.012, 2016.

Smedley, A. R. D., Evatt, G. W., Mallinson, A., and Harvey, E.: Solar radiative transfer in Antarctic blue ice: spectral considerations, subsurface enhancement, inclusions, and meteorites, The Cryosphere, 14, 789–809, https://doi.org/10.5194/tc-14-789-2020, 2020.

Tubini, N., Gruber, S., and Rigon, R.: A method for solving heat transfer with phase change in ice or soil that allows for large time steps
645 while guaranteeing energy conservation, The Cryosphere, 15, 2541–2568, https://doi.org/10.5194/tc-15-2541-2021, 2021.

Vincent, C., Gilbert, A., Jourdain, B., Piard, L., Ginot, P., Mikhalenko, V., Possenti, P., Le Meur, E., Laarman, O., and Six, D.: Strong changes in englacial temperatures despite insignificant changes in ice thickness at Dôme du Goûter glacier (Mont Blanc area), The Cryosphere, 14, 925–934, https://doi.org/10.5194/tc-14-925-2020, 2020.

Vionnet, V., Brun, E., Morin, S., Boone, A., Faroux, S., Le Moigne, P., Martin, E., and Willemet, J.-M.: The detailed snowpack scheme Crocus
650 and its implementation in SURFEX v7.2, Geoscientific Model Development, 5, 773–791, https://doi.org/10.5194/gmd-5-773-2012, 2012.

Vionnet, V., Guyomarc'h, G., Naaim Bouvet, F., Martin, E., Durand, Y., Bellot, H., Bel, C., and Puglièse, P.: Occurrence of blowing snow events at an alpine site over a 10-year period: Observations and modelling, Advances in Water Resources, 55, 53–63, https://doi.org/10.1016/j.advwatres.2012.05.004, 2013.

Washburn, B.: Mapping Mount Everest, Bulletin of the American Academy of Arts and Sciences, 42, 29–44,
655 https://doi.org/10.2307/3824352, 1989.

Zemp, M., Huss, M., Thibert, E., Eckert, N., McNabb, R., Huber, J., Barandun, M., Machguth, H., Nussbaumer, S. U., Gärtner-Roer, I., Thomson, L., Paul, F., Maussion, F., Kutuzov, S., and Cogley, J. G.: Global glacier mass changes and their contributions to sea-level rise from 1961 to 2016, Nature, https://doi.org/10.1038/s41586-019-1071-0, 2019.
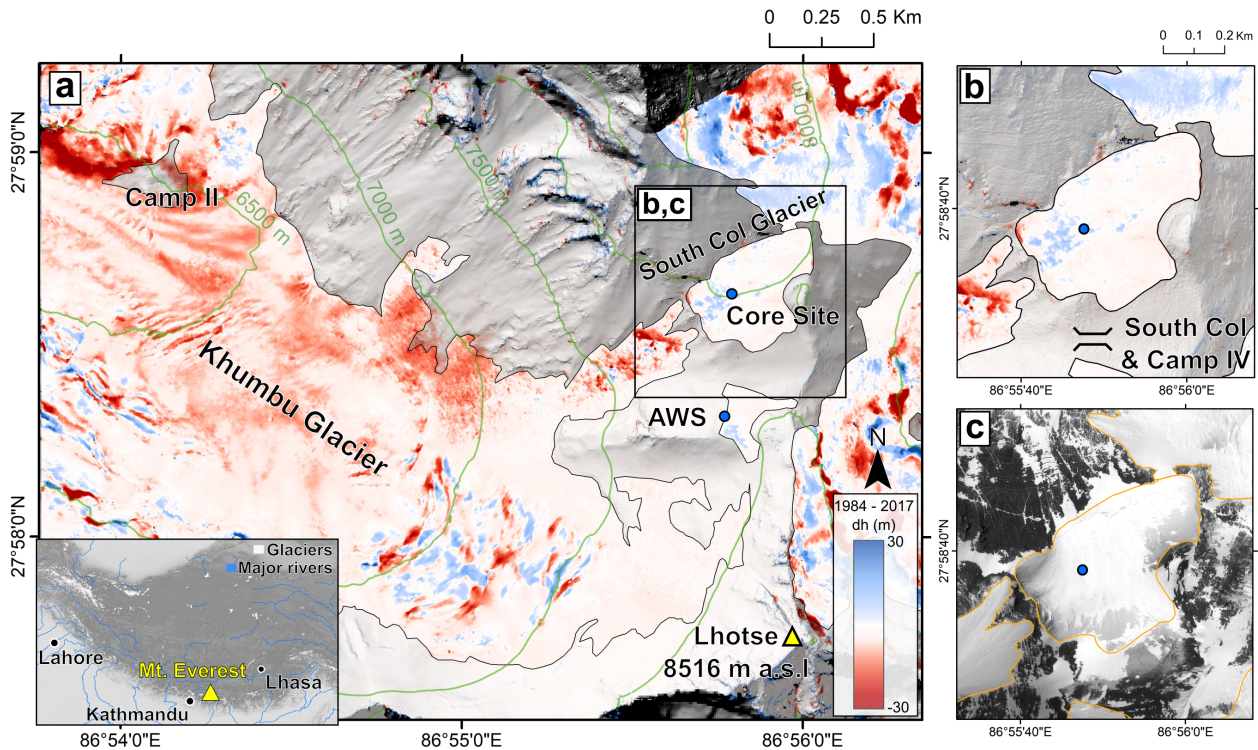
Figure 1. Surface elevation change over the Western Cwm (a) between 1984 and 2017, and over the South Col Glacier (b). The location of the ice core and AWS from Potocki et al. (2022) are shown with blue dots. Background is a shaded relief from the Pléiades DEM. The conditions at the surface of the South Col Glacier on ~~the~~ 23 March 2017 are captured by a Pléiades orthoimage in panel c~~(~~. Pléiades, copyright CNES 2017, Distribution Airbus DS~~)~~. Elevations are reported relative to the geoid. The inset in panel a shows the location of Mount Everest

~~Pléiades orthoimage of South Col Glacier (23 March 2017), showing the location of some remarkable features. A tentative accumulation area of South Col Glacier is highlighted with dots. The dashed line is the separation between the accumulation and ablation area, along which the ice flux Φ is calculated. Red arrows show the direction of the ice flux. The shaded hashed area represent glacierized area that might belong to South Col Glacier, but it is not possible to conclude solely from satellite imagery. Contour lines in gray are plotted every 10 m and extracted from the Pléiades DEM, the elevation corresponds to height relative to the ellipsoid WGS84. Pléiades, copyright CNES 2017, Distribution Airbus DS.~~

660
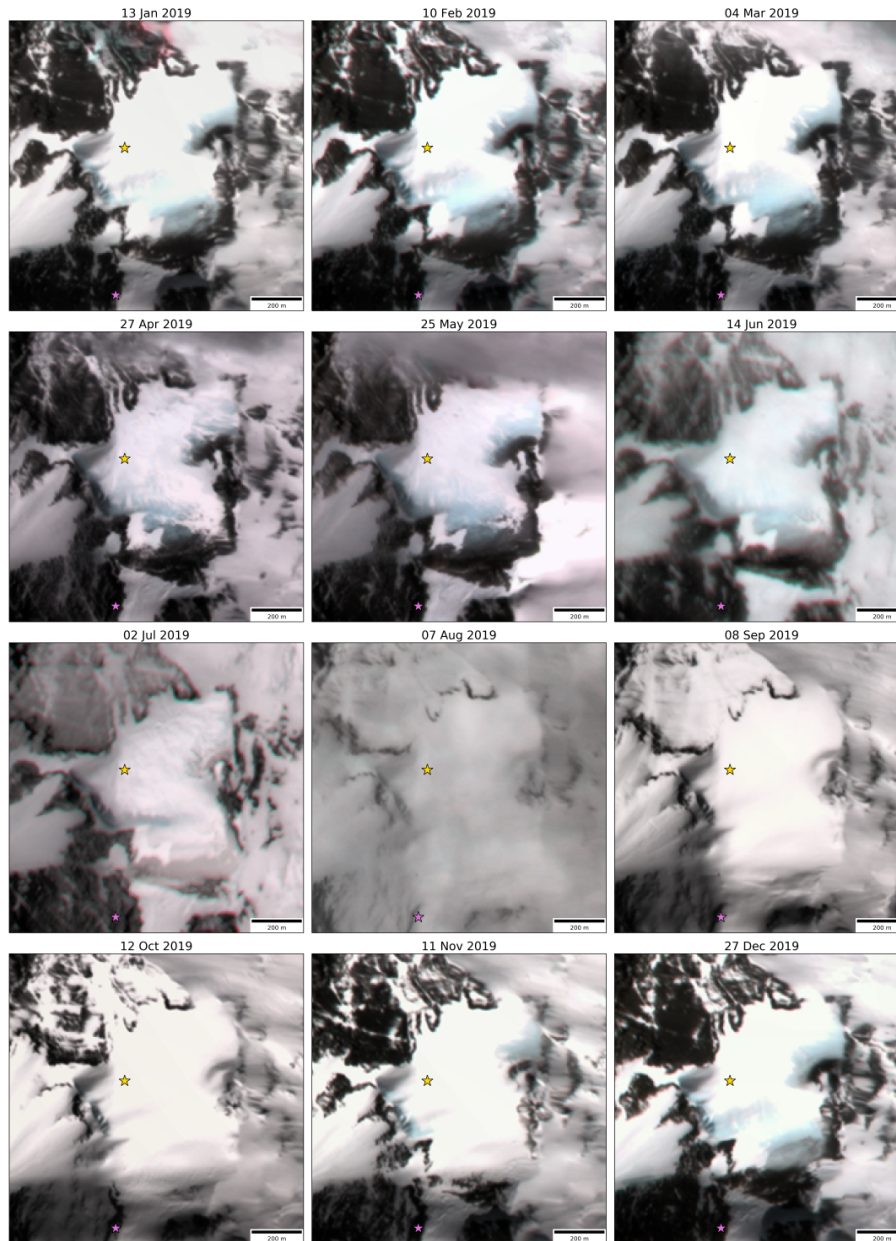
Figure 2. Natural color composites (bands 7-4-3) of VENµS images (CC BY-NC 4.0) showing the seasonal variability of the surface snow cover of South Col Glacier. The yellow star shows the location of the drilling site and the purple one, the location of the South Col AWS. Note the striking expansion of blue ice areas outside the monsoon months, i.e. Oct. – Dec. 2019, or Jan. – April 2019.
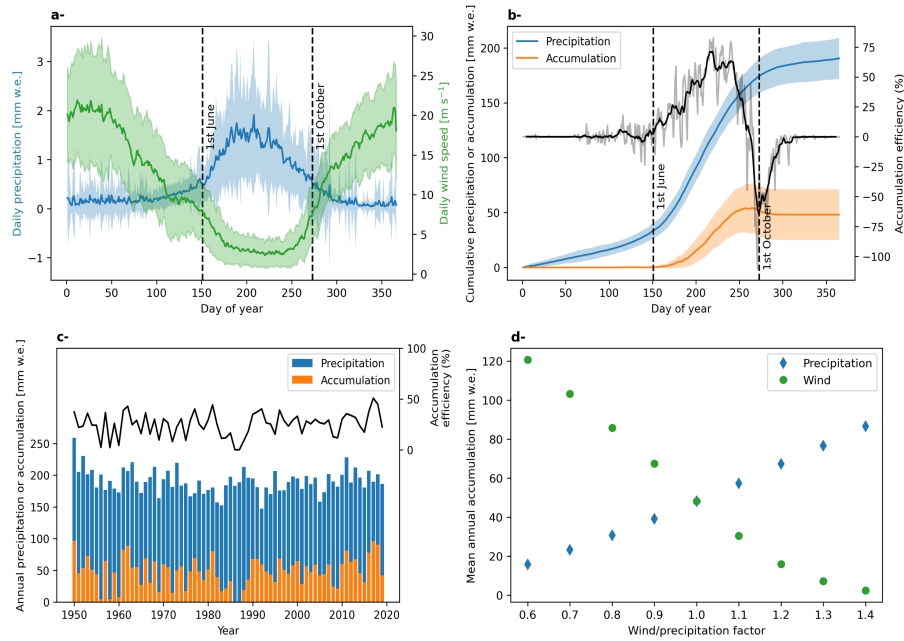
Figure 3. Seasonal cycle of wind and precipitation from downscaled ERA5 data (a) and cumulative precipitation/~~deposition~~ accumulation from the wind erosion model (b) for the period 1950-2020. The black curve on panel b shows the 9 day moving average of the daily ratio of ~~deposition~~ accumulation over precipitation. Panel c shows the annual values of precipitation, ~~deposition~~ accumulation and ~~deposition~~ accumulation efficiency. The model sensitivity to the wind and precipitation factors is shown on panel d, where the averages are calculated for the period 1950-2020.
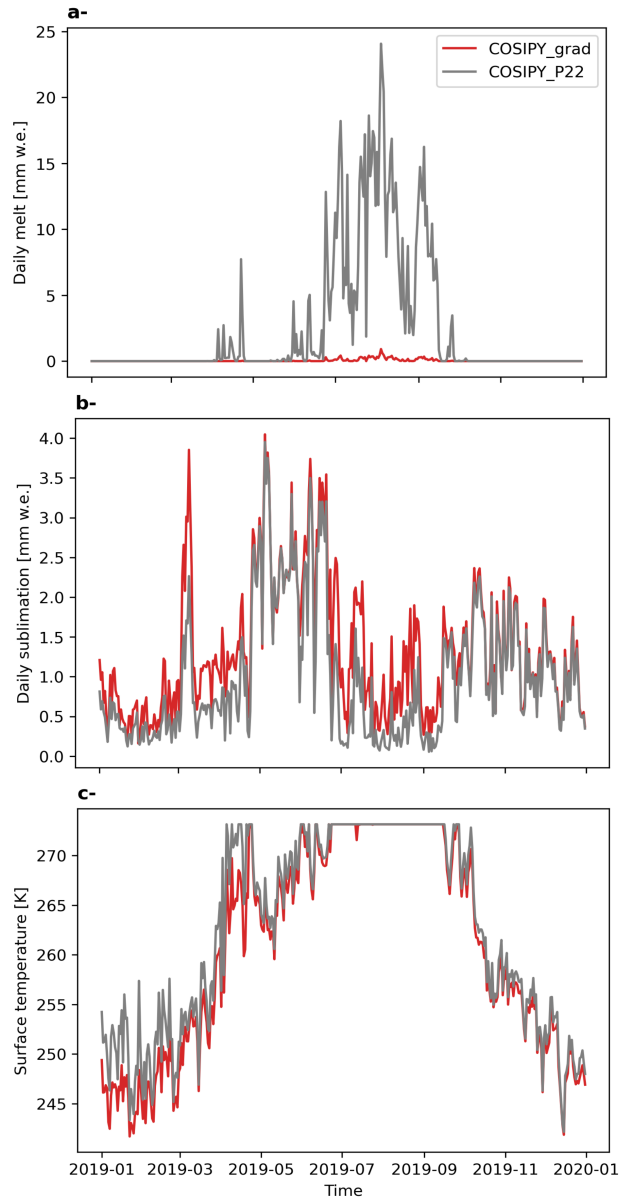
Figure 4. Daily melt rate (a), sublimation rate (b) and ~~maximum daily~~ surface temperature (c) simulated by ~~COSIPY_~~P22 (~~dashed blue~~grey) ~~, and~~ COSIPY_grad (~~blue~~red) ~~and Crocus (orange)~~ models for the year 2019. Daily ~~ablation~~ rates are computed from the hourly sum. The daily surface temperature corresponds to the maximum simulated during the day. Note that the initial thermal state is identical for ~~these three simulation~~ all simulations and is ~~predicted~~ estimated by a COSIPY simulation similar to ~~COSIPY_~~P22, that ran from 2010-01-01 to 2019-01-01.
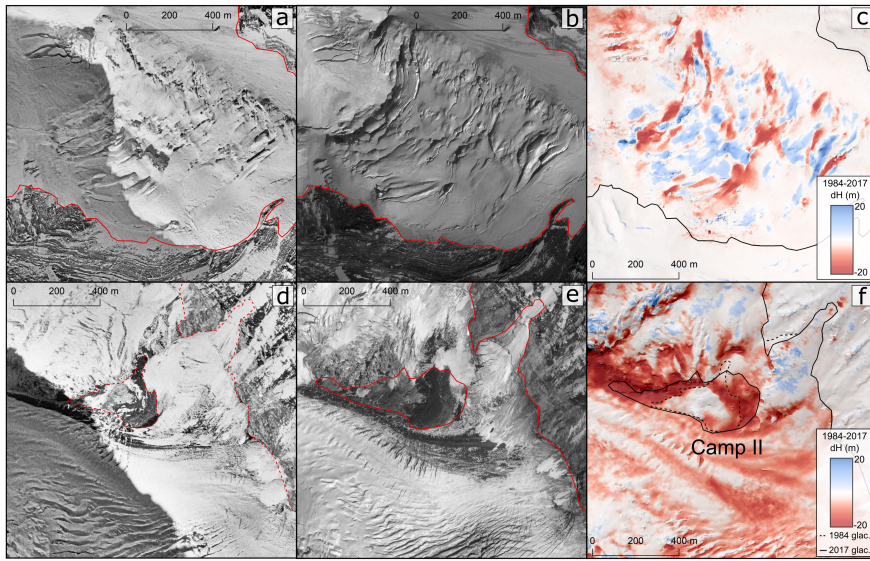
Figure A1. Examples of glacier surface conditions captured by aerial photographs (1984) and Pléiades imagery (2017) in the Western Cwm and associated changes in surface elevation. Top row: Crevassing of the Lhotse face in 1984 (a) and 2017 (b) and corresponding elevation change estimates (c) over the same period. The alternating positive and negative elevation difference pattern reflects the movement, opening and/or closure of crevasses. Bottom row: the expansion of the area of exposed bedrock around Camp II between 1984 (d) and 2017 (e) and associated elevation changes (f). Shadows prominent in panels a and d illustrate the winter time acquisition date of the aerial photographs, compared to the Spring (23rd March) acquisition of the Pléiades imagery (panels b and e). Pléiades, copyright CNES 2017, Distribution Airbus DS.
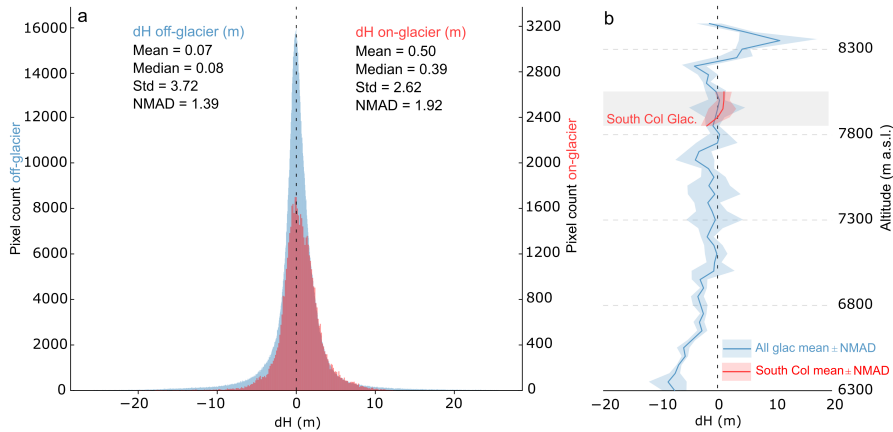
Figure A2. Distribution of the elevation change values off-glacier and on South Col Glacier (a). Elevation changes for 1984-2017 as a function of elevation for every 50 m elevation bin for the whole glacierized area and for South Col Glacier (b).
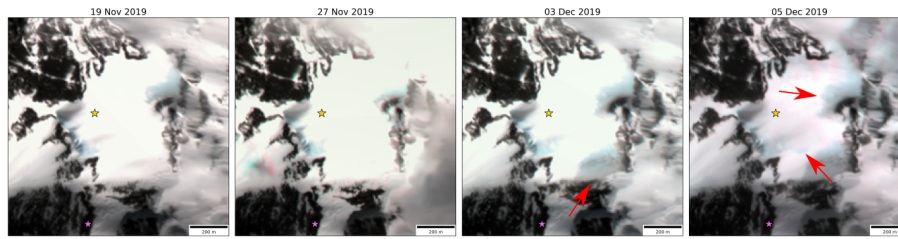
Figure A3. Natural color composites (bands 7-4-3) of VENμS images ~~(CC BY-NC 4.0)~~ showing episodes of snow cover loss in November and December 2019. the yellow star shows the location of the drilling site and the purple one, the location of the South Col AWS. The red arrows point to the area of large changes.
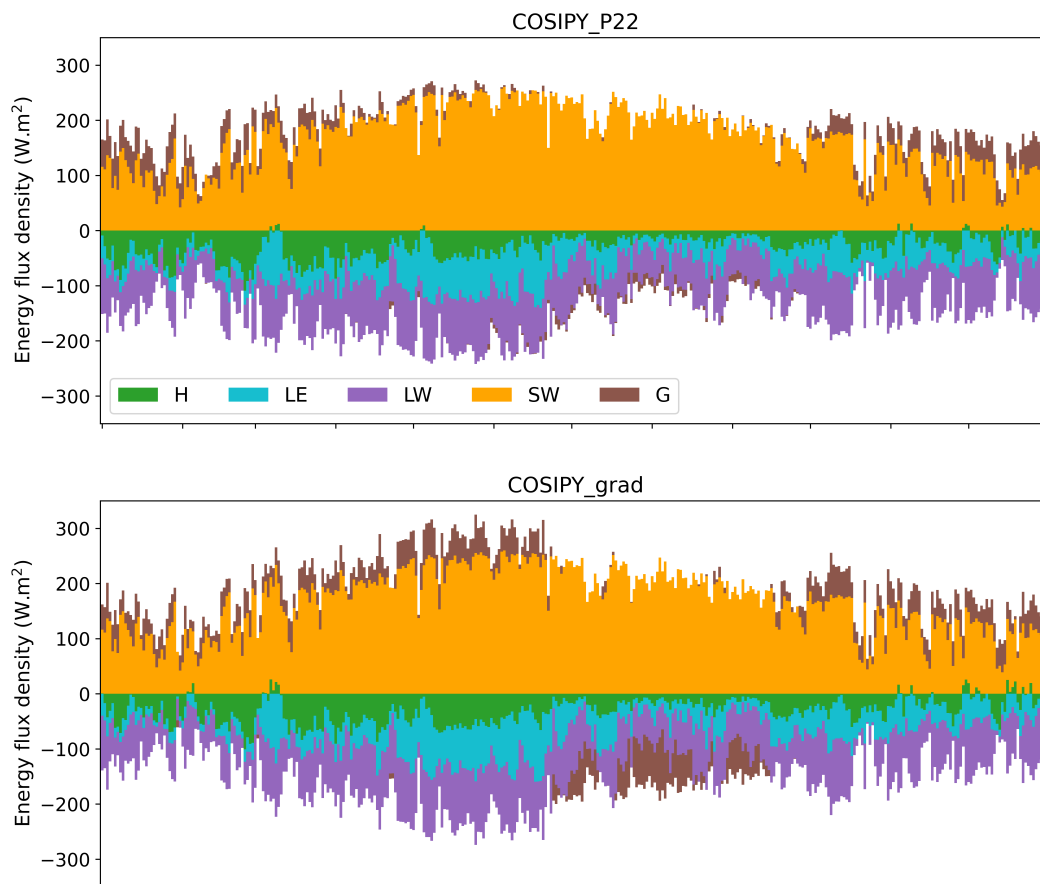
Figure A4. Day-of-year mean energy fluxes for the ice simulations with (a) COSIPY_P22, (b) COSIPY_grad and (c) CROCUS_ice for the year 2019.
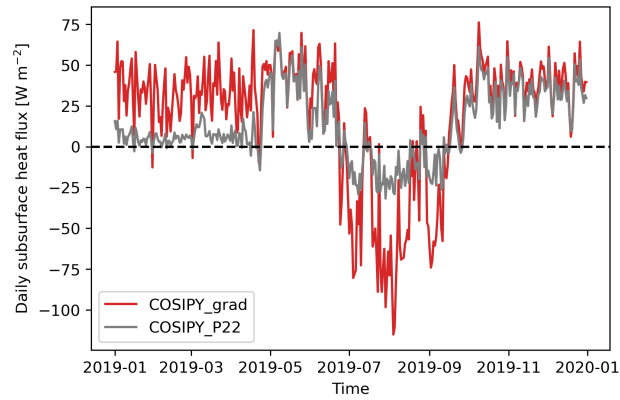
Figure A5. Daily averages of ground heat flux for the COSIPY_P22 and the COSIPY_grad simulations.
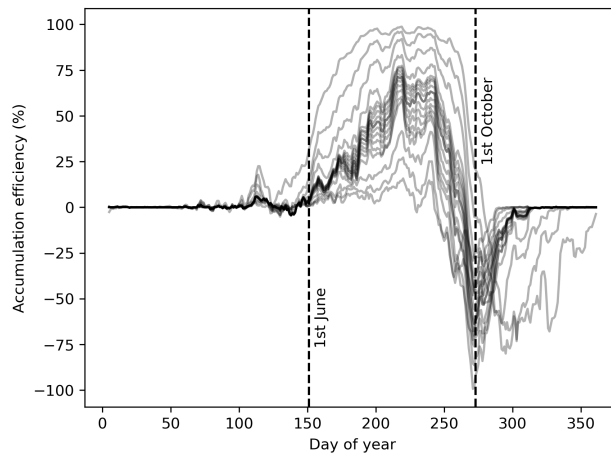
Figure A6. ~~Deposition~~ Accumulation efficiency averaged over the period 1950-2020. Each line represents one simulation with a varying wind or precipitation factor. All the lines are smoothed with a 9 day running mean.
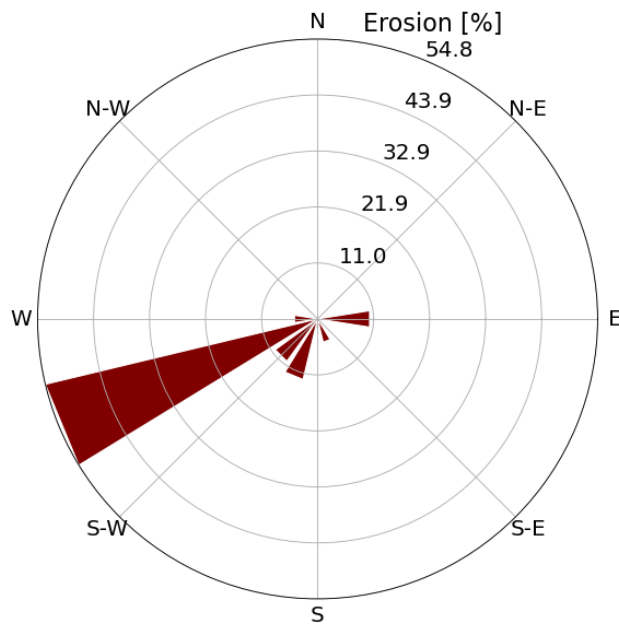
Figure A7. Erosion as a function of wind direction for the period where wind data are available from the AWS, showing the dominant role of WSW winds.